JACS
JOURNAL OF THE AMERICAN CHEMICAL SOCIETY
Article
pubs.acs.org/JACS

How Formaldehyde Inhibits Hydrogen Evolution by [FeFe]-Hydrogenases: Determination by ^{13}C ENDOR of Direct Fe−C Coordination and Order of Electron and Proton Transfers

Andreas Bachmeier,[†] Julian Esselborn,[§] Suzannah V. Hexter,[†] Tobias Krämer,[†] Kathrin Klein,[∥] Thomas Happe,*[,§] John E. McGrady,*[,†] William K. Myers,*[,‡] and Fraser A. Armstrong*[,†]

[†]Inorganic Chemistry Laboratory and [‡]Centre for Advanced Electron Spin Resonance, Department of Chemistry, University of Oxford, South Parks Road, Oxford OX1 3QR, United Kingdom

[§]Lehrstuhl für Biochemie der Pflanzen, AG Photobiotechnologie and [∥]Lehrstuhl für Anorganische Chemie I, Ruhr-Universität Bochum, 44801 Bochum, Germany

Supporting Information

ABSTRACT: Formaldehyde (HCHO), a strong electrophile and a rapid and reversible inhibitor of hydrogen production by [FeFe]-hydrogenases, is used to identify the point in the catalytic cycle at which a highly reactive metal-hydrido species is formed. Investigations of the reaction of *Chlamydomonas reinhardtii* [FeFe]-hydrogenase with formaldehyde using pulsed-EPR techniques including electron−nuclear double resonance spectroscopy establish that formaldehyde binds close to the active site. Density functional theory calculations support an inhibited super-reduced state having a short Fe−^{13}C bond in the 2Fe subsite. The adduct forms when HCHO is available to compete with H^+ transfer to a vacant, nucleophilic Fe site: had H^+ transfer already occurred, the reaction of HCHO with the Fe-hydrido species would lead to methanol, release of which is not detected. Instead, Fe-bound formaldehyde is a metal-hydrido mimic, a locked, inhibited form analogous to that in which two electrons and only one proton have transferred to the H-cluster. The results provide strong support for a mechanism in which the fastest pathway for H_2 evolution involves two consecutive proton transfer steps to the H-cluster following transfer of a second electron to the active site.

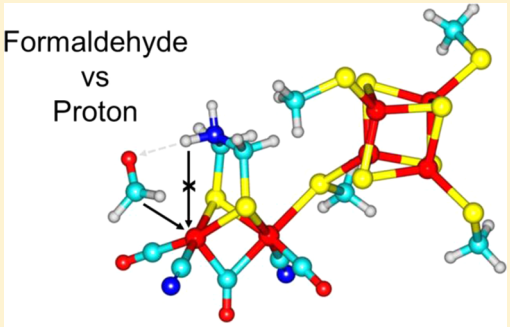

INTRODUCTION

The enzymes known as [FeFe]-hydrogenases (H2ases) are superb catalysts for hydrogen production from water: they serve as benchmarks for what must be achievable with synthetic catalysts composed of first-row d-block elements, both in terms of high turnover frequency, turnover number, and low overpotential requirements. The active site, known as the H-cluster, is highly conserved among the different [FeFe]-H2ases and consists of a binuclear iron subcluster $[2Fe]_H$ that is connected, via a cysteine sulfur ligand, to a cubane $[4Fe\text{-}4S]_H$ cluster (see Scheme 1).[1] The Fe atoms in $[2Fe]_H$, designated "distal" (Fe_d) or "proximal" (Fe_p) according to their position with respect to the $[4Fe\text{-}4S]_H$ domain are each coordinated by CO and CN^- ligands and are bridged by an unusual aza-dithiolate (adt) ligand that positions a pendant amine-N above Fe_d.[1] Aside from an inactive oxidized form known as H_{ox}^{inact}, in which both Fe atoms of $[2Fe]_H$ are Fe(II) and the $[4Fe\text{-}4S]_H$ domain is oxidized (2+), three active oxidation levels of the H-cluster have been identified by spectroscopy: H_{ox}, H_{red}, and a "super-reduced" state known as H_{sred}.[1] Carbon monoxide, a potent inhibitor of [FeFe]-hydrogenases, binds strongly to H_{ox}, and X-ray crystallography shows that CO binds to Fe_d.[2] It follows that Fe_d is most likely the site at which H_2 binds. Carbon monoxide binds less strongly to H_{red} (it destabilizes the H-cluster)[3] and does not bind to H_{sred}.[4] The fact that CO protects against irreversible inactivation by O_2 has been interpreted in terms of O_2 also binding, initially, at Fe_d,[5,6] leaving an inactive $[4Fe\text{-}4S]_H$ domain that can be reactivated *in vitro*.[7]

Studies of [FeFe]-hydrogenases by protein film electrochemistry (PFE) have established them to be reversible electrocatalysts, switching immediately between H_2 production and H_2 oxidation as the electrode potential is scanned across the reversible hydrogen electrode potential. Previously,[4] we distinguished the steady-state redox-levels of the H-cluster dominating at different potentials as H_{ox}, H_{ox-1}, and H_{ox-2}, rather than using the spectroscopic labels H_{red} and H_{sred}. We retain our electrochemical nomenclature here, as it allows us to discriminate between catalytic oxidation levels that have clear overall electronation states, but may have different protonation states.

Scheme 1 draws attention to an outstanding question concerning the mechanism of H_2 activation. Of the two

Received: December 23, 2014
Published: April 14, 2015

DOI: 10.1021/ja513074m
J. Am. Chem. Soc. 2015, 137, 5381−5389

Scheme 1. Pathway to the Transient Precursor for Catalytic H_2 Formation at the H-Cluster, Formation of Which Is Prevented by Formaldehyde[a]

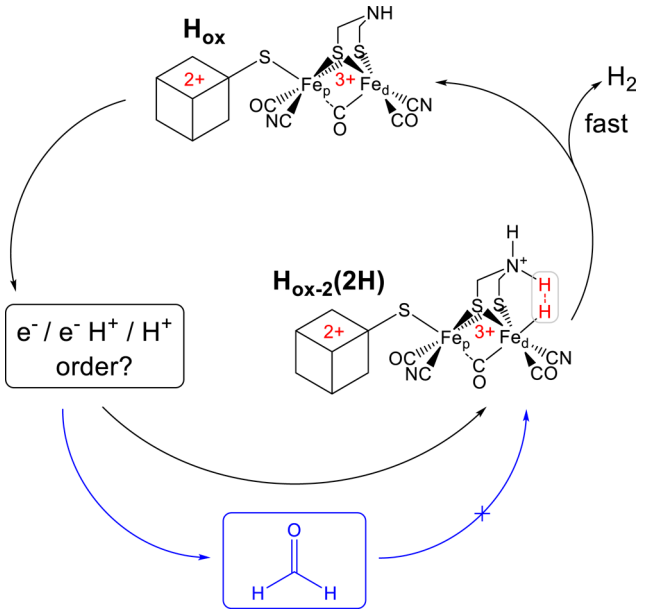

[a]As the individual charges on Fe_p and Fe_d are still under debate, the overall oxidation number of $[2Fe]_H$ is presented, together with the charge of $[4Fe\text{-}4S]_H$. In H_{ox}, $[4Fe\text{-}4S]_H$ is established to have an overall charge of 2+, and both $Fe_p(I)\text{-}Fe_d(II)$ and $Fe_p(II)\text{-}Fe_d(I)$ are possible combinations for $[2Fe]_H$. In $H_{ox-2}(2H)$, $[4Fe\text{-}4S]_H$ is also formulated as 2+,[8] implicating that $[2Fe]_H$ comprises $Fe_p(I)\text{-}Fe_d(II)$.[1]

structures shown, H_{ox} is well characterized; the other structure represents a transient state, termed $H_{ox-2}(2H)$, immediately prior to or at the point of H_2 release. To go from H_{ox} to $H_{ox-2}(2H)$ requires two electrons and two protons, but it has not been established, experimentally and in a kinetic study, in which order these events occur. In the $H_{ox-2}(2H)$ transient, the two additional electrons (with respect to H_{ox}) are stored as a terminal hydride bound to Fe_d; therefore, the oxidation numbers of the H-cluster components $[2Fe]_H$ and $[4Fe\text{-}4S]_H$ are already adjusted to the H_{ox} level, which is left behind after H_2 is released from the active site. The individual oxidation numbers of Fe_d and Fe_p (1,2) are left unassigned. Scheme 1 includes an inhibition step that is the focus of this paper.

Formaldehyde has been identified by PFE to be a potent inhibitor of H_2 evolution by [FeFe]-hydrogenases.[4,9] Importantly, the activity that is lost very rapidly when formaldehyde is injected into the electrochemical cell is recovered immediately when formaldehyde is removed (Figure S1A). Formaldehyde binds rapidly within seconds, the reaction in the potential regime driving H_2 production is dominated by a fast component with τ = 7.89 s at −0.56 V vs SHE (Figure S1B). The enzymatic activity is almost fully recovered when formaldehyde is flushed from the cell after 5 min exposure (Figure S1A).

The fraction of the total current attenuation that is due to rapid, reversible interaction with HCHO increases as the electrode potential is lowered:[9] a detailed study with the enzyme from *Clostridium acetobutylicum* showed that the potential dependence spans three zones linked by one-electron Nernst transitions and thus termed H_{ox}, H_{ox-1}, and H_{ox-2}. Allowing for small shifts, the profile complemented that obtained from inhibition by CO, thus implicating the most reduced catalytic intermediate, two electrons below H_{ox} and hence at the level of H_{ox-2}, as the primary target for rapid and reversible inhibition.[4] Hence, formaldehyde prevents the formation of the transient species $H_{ox-2}(2H)$ depicted in Scheme 1 (blue pathway). A much slower reaction, which is not reversible, is also observed and becomes dominant as the electrode potential is raised.[4,9] However, the fact that at negative potentials where H_{ox-2} prevails, the rapidly inhibited fraction is almost quantitatively recovered upon formaldehyde removal after 5 min (Figure S1A) means that the fast binding process offers substantial protection against the slow and irreversible reaction.

Based on earlier evidence from density functional theory (DFT)[8,10,11] that in the H_{sred} state (and likely also H_{red}) Fe_d should carry a hydrido-ligand, we originally proposed that HCHO inhibition of the H_{ox-1} and H_{ox-2} levels occurs, mechanistically, through electrophilic attack on the respective hydrido complex to form a bound methanol or methoxide species.[4] However, subsequent efforts to detect any release of methanol have been unsuccessful,[4,12] implying that HCHO is binding as a true inhibitor and is not an alternative, slow substrate. Further, results from spectroscopic investigations by different groups have led to the proposal that Fe_d carries a hydrido ligand neither in H_{red}[13,14] (H_{ox-1} level) nor in the spectroscopically accessible form of H_{sred} (H_{ox-2} level);[15] the implication being that H_2 evolution occurs very rapidly following transfer of two protons upon the transition to or at the H_{ox-2} redox level.[1] These developments now place the nature of the reaction with formaldehyde, which contains a potent electrophilic C atom, in a new context, namely, as a probe to investigate when the initial H^+ transfer to Fe_d (to form the hydrido complex) occurs during catalysis as well as the subsequent second protonation of the adt moiety. The results also convey additional structural information, because known complexes of metals with formaldehyde do not only bind through a single metal-C bond but also involve secondary stabilization through di-hapto (η-C,O) coordination,[16−18] a notable example being $Fe(\eta^2\text{-}CH_2O)(CO)_2(P(OMe)_3)_2$ reported by Berke et al.[19]

We have now undertaken pulsed-EPR spectroscopy experiments with isotopically enriched formaldehyde (DCDO and $H^{13}CHO$) to gain insight into the binding mode of formaldehyde to the H-cluster in *Cr*HydA1 from the green alga *Chlamydomonas reinhardtii*. The H-cluster in *Cr*HydA1 is structurally identical to its homologues, but spectra are not complicated by the additional FeS clusters that are present in other [FeFe]-H2ases. The H_{ox-2} level of *Cr*HydA1, which is easily generated by placing the enzyme under a H_2 atmosphere, is thus amenable to detailed EPR spectroscopic characterization, in contrast to the other [FeFe]-H2ases.[15,20] Use of EPR allows the species formed upon rapid and reversible reaction with formaldehyde to be studied over long periods in frozen samples, avoiding the irreversible degradation that would inevitably result from using techniques such as IR that normally require ambient temperatures. The results have important implications for the mechanism of [FeFe]-H2ases.

MATERIALS AND METHODS

All chemicals were used as purchased without further purification. Phosphate buffer was made up of NaCl, NaH_2PO_4, and Na_2HPO_4 (analytical reagent grade, Sigma-Aldrich), 10% (v/v) glycerol, and titrated to pH 6.0. Aldehydes used in this work were purchased from

DOI: 10.1021/ja513074m
J. Am. Chem. Soc. 2015, 137, 5381−5389

Sigma-Aldrich: formaldehyde-d_2 solution (~20 wt % in D_2O, 98 atom % D) and formaldehyde-^{13}C solution (20 wt % in H_2O, 99 atom % ^{13}C).

Experiments were conducted with hydrogenase *Cr*HydA1 from the green alga *C. reinhardtii*,[1,21] isolated as apoprotein lacking the $[2Fe]_H$ subcluster via strep-tactin affinity chromatography from heterologous expression in *E. coli* as described previously.[22−24] The protein was maturated *in vitro* with the complex $Fe_2[\mu\text{-}(SCH_2)_2NH](CN)_2(CO)_4^{2-}$ and subsequently purified using a NAP 5 gel filtration column (GE Healthcare) and concentrated using Amicon Ultra centrifugal 10 K filters (Millipore) as shown before.[25] The total protein concentration (2.4 mM) was estimated spectroscopically using the method of Bradford,[26] with bovine serum albumin (Sigma-Aldrich) as the protein standard; protein purity was assessed by SDS-PAGE. The H_2 evolution activity of *Cr*HydA1 was measured as 1.37 mmol H_2 min^{-1} mg^{-1} in a well-established assay with methyl viologen as electron mediator and detection of H_2 via GC.[27] Isolation, handling, and storage of the protein were conducted under strictly anaerobic conditions. Protein samples were stored at −80 °C before preparation for EPR. All EPR samples were prepared in an anaerobic glovebox (O_2 < 3 ppm) in 50 mM phosphate buffer containing 0.1 M NaCl, 10% (v/v) glycerol, adjusted to pH 6.0 at 20 °C. All samples were prepared in 3.0 mm high-precision EPR tubes (Wilmad 706-PQ-9.50) to ensure accurate spin quantification.

EPR samples were prepared by reducing approximately 70 μL of as-isolated enzyme using 100% H_2 at 20 °C under zero-current flow until the potential of the solution equilibrated, typically after 3.5 h. Formaldehyde (DCDO or $H^{13}CHO$) was then injected to give a final concentration of free, nonhydrated aldehyde (the equilibrium constant for hydration K_{eq}(hydration) ≈ 2000 at 25 °C)[28,29] equal to the concentration of *Cr*HydA1. Aliquots (ca. 70−90 μL) of the resulting solution were transferred as quickly as possible to Wilmad EPR tubes and frozen in liquid nitrogen, i.e., within 5 min after injection, a time scale after which almost all enzymatic activity was noted to be recovered in PFE experiments (Figure S1A). Spin quantification was carried out using copper perchlorate samples (50 μM $CuSO_4$ in 2 M $NaClO_4$ (aq) adjusted to pH 1.22 with HCl) measured under nonsaturating conditions.

Continuous wave (CW) EPR experiments were performed using an X-band (ca. 9.4 GHz) Bruker EMX^{micro} premium spectrometer (Bruker BioSpin GmbH, Germany) with an X-band SHQE-W cylindrical TE_{011}-mode resonator (Bruker). Background spectra of the empty resonator were recorded under identical conditions and subtracted from the EPR spectrum of the enzyme sample. Pulse measurements were carried out on an X-/W-band Bruker Elexsys 680 spectrometer and a Q-band Bruker Elexsys 580 spectrometer.

Spectroscopic simulations were performed in MATLAB 2013a with the EasySpin 4.5 toolbox.[30] Simulation of the FID-detected EPR signal employed matrix diagonalization with the pepper function using a *g*-strain model for line width, as is characteristic for simulations of FeS cluster EPR signals. The EPR fit was then converted to an equivalent line width defined by hyperfine broadening, "H-Strain", and this set of EPR simulation parameter values acted as a basis for Mims ENDOR simulations making use of the saffron function with explicit use of the experimental parameter values.

All DFT calculations reported in this paper were performed using the Gaussian 09 suite. The basic structure of the H-cluster was extracted from the reported crystal structure of *Delsulfovibrio desulfuricans* (pdb code 1HFE)[31] following the procedure set out by Bruschi et al.[8] The active site was extracted from the protein matrix, and the oxygen atom originally assigned in the bridging position was replaced with a CO unit. The H-cluster is attached to the protein via four cysteine units (cys179, cys234, cys378, and cys382); all four were modeled as CH_3S units, with the carbon atoms frozen at the positions found in the matrix. All other structural parameters were freely optimized. Given the uncertainty in the position of the bridging CO ligand we initialized optimizations from a number of starting geometries where the CO is bridging, semibridging, or terminal. In all cases the CO reverts to the bridging position in the optimized structure. At the H_{ox-2} oxidation level the total charge on the cluster is −5, decreasing to −4 when the system is protonated, as in the $[tH\text{-}dtma]^{4-}$ structure reported by Bruschi et al.[8] The stabilizing influence of the wider protein matrix was introduced through a polarized continuum model with dielectric constant ε = 4.0. The majority of the calculations were performed with the BP86 functional[32,33] along with a triple-ζ quality basis set (Ahlrich's TZVP)[34] on all atoms. The dependence of the spin density distribution on methodology was also explored, using the B3LYP[35] functional. These latter calculations were done as single points using the geometries optimized at the BP86/TZVP level. The exchange coupling within the $[4Fe\text{-}4S]_H$ cluster (and also, in principle, within the $[2Fe]_H$ catalytic unit) was treated using the broken-symmetry approach, wherein opposing spin moments are imposed on the initial (guess) spin density, such that the system converges to a predominantly antiferromagnetic state. In all cases here, the antiferromagnetic species has an M_S = 1/2 ground state, which can be formulated to a first approximation in terms of a reduced $[4Fe\text{-}4S]^{1+}$ cluster. Appropriately spin-polarized initial guesses were constructed using the "guess = fragment" keyword available in Gaussian 09.[36] Calculations were initialized using a wide range of initial spin densities corresponding to ferro/antiferromagnetic coupling within the $[4Fe\text{-}4S]_H$ cubane and also to ferro/antiferromagnetic coupling of the spin densities on the $[2Fe]_H$ unit. A range of initial guesses was constructed in which the extra electron starts (a) on the $[4Fe\text{-}4S]_H$ unit and (b) on the $[2Fe]_H$ catalytic unit. The converged wave function for the one-electron oxidized case (where the oxidation states are unambiguous) was also used as an initial guess. In no case did we find that the initial guess has a significant impact on the converged results; the self-consistent density (*vide infra*) is essentially identical. Moreover, in no case did we find evidence for antiferromagnetic coupling (i.e., opposing spin densities) on the $[2Fe]_H$ unit in the converged self-consistent solution. Mulliken spin densities on Fe_d and Fe_p are always small (<0.25 electrons) and have the same sign.

RESULTS

EPR Spectroscopy. Figure 1 shows the integrated free-induction decay (FID) X-band EPR spectrum of H_2-reduced *Cr*HydA1 in the presence of formaldehyde. The sample was equilibrated in an anaerobic glovebox under H_2 flow for 3.5 h before formaldehyde was injected into the enzyme solution to give a final concentration of free (i.e., nonhydrated)[9] HCHO equal to the concentration of *Cr*HydA1. The spectrum features a rhombic system consistent with a reduced cubane cluster

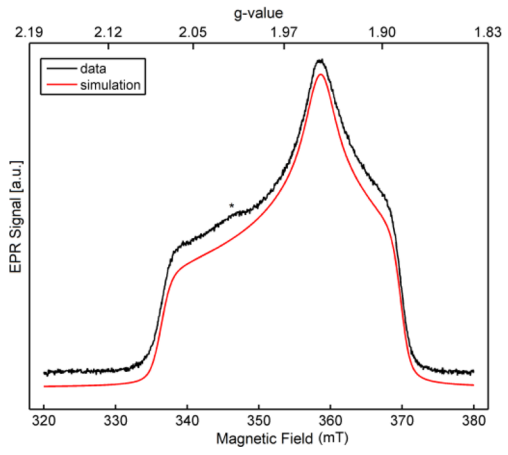

Figure 1. X-band FID-detected EPR spectrum at 10 K, black, and a simulation, red, of formaldehyde-inhibited *Cr*HydA1, at a spin concentration of 830 μM. The π/2 pulse length was 320 ns. Simulation values were g_x = 2.074, g_y = 1.946, and g_z = 1.886. A degradation product is indicated (*).

DOI: 10.1021/ja513074m
J. Am. Chem. Soc. 2015, 137, 5381−5389

($[4Fe\text{-}4S]^{1+}$),[37] meaning that the great majority of spin-density resides on $[4Fe\text{-}4S]_H$. By EPR simulation, the g values are 2.074, 1.946, and 1.886, which agree with those observed previously for H_{ox-2}.[15,20] The minor signal at g = 2.025 most likely corresponds to a slowly formed decay product following HCHO inhibition of *Cr*HydA1. This observation is consistent with PFE results, where small proportions of slow, irreversible inhibition are observed when *Cr*HydA1 is subjected to HCHO at negative potentials (even though fast, reversible inhibition is the dominant pathway).[12]

To characterize the formaldehyde interaction with the H-cluster, pulsed-ENDOR spectra of ^{13}C-labeled HCHO were recorded at Q-band for several g values, as shown in Figure 2.

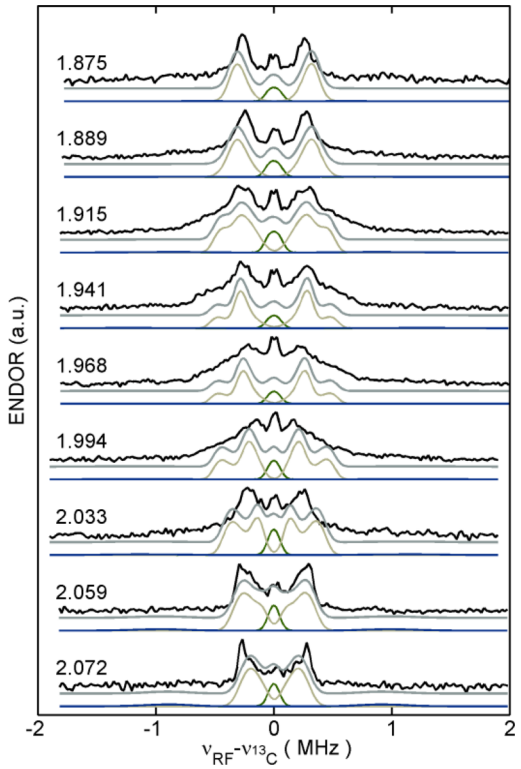

Figure 2. Q-band Mims ENDOR spectra (black) and simulations of $H^{13}CHO$ inhibited *Cr*HydA1 recorded at several g values, as indicated. For all traces the temperature was 8 K, with a τ value of 250 ns, π(RF) = 80 μs, repetition time of 20.4 ms, and microwave frequency was 33.7704 GHz.

The observed ENDOR frequencies for the hyperfine interaction (A) of $A/2$ less than the nuclear Larmor frequency are

$$\nu^{\pm}_{ENDOR}(^{13}C) = \nu(^{13}C) \pm |A(^{13}C)|/2 \quad (1)$$

Here, $\nu(^{13}C)$ is the nuclear Larmor frequency, and $A(^{13}C)$ is the hyperfine interaction value for an arbitrary orientation of the electron−nucleus vector in the magnetic field.

The ENDOR data were analyzed with the following:

$$\mathbf{A} = a_{iso}\mathbf{1} + \mathbf{gT}/g_e \quad (2)$$

where $\mathbf{A}$ is the full hyperfine tensor, a_{iso} is the isotropic value of $\mathbf{A}$, defined as its mean, $\mathbf{1}$ is the identity matrix, and $\mathbf{T}$ is the dipolar component for the nucleus which is scaled by the effective g value, $\mathbf{g}/g_e$. In the principle axis of a point−dipole interaction:

$$\mathbf{T} = \frac{\mu_0}{4\pi\hbar}\frac{g_e\beta_e g_n\beta_n}{R^3}\rho_{Fe}[-1 \quad -1 \quad 2] = [-T \quad -T \quad 2T] \quad (3)$$

Here, one sees that the dipolar interaction is proportional to the spin density of the Fe center ρ_{Fe}/R^3, and this could be appropriate for coordination at the distal Fe, more than 8 Å away from the spin-bearing $[4Fe\text{-}4S]_H^{1+}$ subsite. However, for a mixed-valence metal cluster, T is a summation of dipolar interactions of all spin densities with a given nucleus. While full characterization of such a model[38] is beyond the scope of the present work, the local spin model is sufficiently accurate to test trial locations for the coordination of HCHO in the presence of the $[4Fe\text{-}4S]_H^{1+}$ subdomain and $[2Fe]_H$. The main points of interest are those sites able to undergo nucleophilic attack at the carbonyl carbon of formaldehyde, such as the terminal position at the distal Fe as shown in Scheme 2, the amine of the azadithiolate (adt) bridge, and the bridging CO position, which has been alternatively suggested to be a μ-hydrido form of H_{ox-2}, separate from the catalytic H_{sred} state.[14] For these calculations, an approximate local spin model is developed.

Scheme 2. Labels of Fe Atoms (1−4, p, d) and g Tensor Alignments (A, B, C) Used in Dipolar Model Calculations and a Putative Location for Bound Formaldehyde (^{13}C)[a]

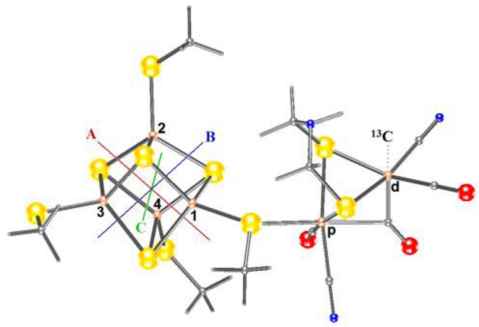

[a]Sulfur atoms are yellow, protons are white, carbon is gray, oxygen is red, nitrogen is blue, and iron is brown.

The dipolar coupling tensor, $\mathbf{T}$, is expanded from eq 3 to include the spin projection factors with the following:

$$\mathbf{A} = a_{iso}\mathbf{1} + \left(\frac{\mu_0 g_e \mu_B g_N \mu_N}{4\pi\hbar}\right) \times \sum_i^6 k'_i \frac{(\mathbf{1} + \Delta\mathbf{g}_i/g_e)}{r_i^5} \begin{bmatrix} r_i^2 - 3x_i^2 & -3x_i y_i & -3x_i z_i \\ -3x_i y_i & r_i^2 - 3y_i^2 & -3y_i z_i \\ -3x_i z_i & -3y_i z_i & r_i^2 - 3z_i^2 \end{bmatrix} \quad (4)$$

In the molecular frame, the dipolar orientation is described directly from the ^{13}C nucleus-to-metal nucleus unit vector $\vec{r}_i = [x_i, y_i, z_i]$, taken here as the nucleus positions rather than the average molecular orbital position.[39] The $\Delta\mathbf{g}_i$ matrix ($\Delta\mathbf{g} = \mathbf{g} - g_{iso}\mathbf{1}$) is defined as the $\mathbf{g}$ tensor of the local spin, i, rotated into the molecular frame. The $\mathbf{g}$ tensor orientation for a $[4Fe\text{-}4S]^{1+}$ cluster is commonly oriented along face normals of the distorted [4Fe-4S] cube (i.e., stellated tetrahedron), however in some cases the g tensor is rotated by 45° along one of these facial vectors.[40] The spin of the iron centers is weighted according to their spin projection factors, k. For the calculations

DOI: 10.1021/ja513074m
J. Am. Chem. Soc. 2015, 137, 5381−5389

here, only the total spin state, $|9/2|4|1/2\rangle$ is considered, which is the spin coupling of ferromagnetic $Fe^{2.5+}$-$Fe^{2.5+}$, $S = 9/2$, and Fe^{2+}-Fe^{2+}, $S = 4$, with total spin of $S_T = 1/2$, and these centers are calculated to have $k(Fe^{2.5+}) = 1.83$ and $k(Fe^{2+}) = -1.33$.[41]

With the spin densities on the proximal and distal irons, of $\rho_p = 0.23$ and $\rho_d = 0.09$, from DFT calculations (*vide infra*), the spin projection factors, k, are scaled to an effective value, k', due to delocalization of spin over the $[2Fe]_H$ subdomain. Delocalization over the low-spin d^6 irons is treated with respect to their coordinated spin center on the $[4Fe\text{-}4S]_H^{1+}$ subdomain. For Fe_1 and Fe_2 of Scheme 2 being $Fe^{2.5+}$ and $\rho = 6.5$, delocalization over Fe_p and Fe_d would lead to $k' = 1.74$ for Fe_1 and Fe_2 and $k' = 0.065$ and $k' = 0.025$ for Fe_p and Fe_d, respectively.[38] Reported values of k for the $Fe^{2.5+}$ vary by up to 15% depending on extent of delocalization and the nature of the spin coupling in the $[4Fe\text{-}4S]^{1+}$ cluster,[41] and these values may be determined experimentally.[42]

To measure the hyperfine interactions of the $H^{13}CHO$ with the H_{ox-2} sample, ENDOR data were collected at X-band and Q-band, along with X-band HYSCORE, and X-band ESEEM of DCDO. Mims ENDOR measurements performed at Q-band afford increased orientation selection and separate the ^{13}C Larmor frequency from overlapping ^{14}N frequencies that are of concern at X-band. At the extreme g values, the single-crystal-like spectra provide the highest resolution of different classes of ^{13}C. Formaldehyde that is remote from Fe_d is seen in the center of the spectrum as a small peak that is somewhat suppressed with a τ value of 250 ns (Figure 2). This signal does not stem from naturally occurring ^{13}C atoms in the protein close to the active site (as, for example, observed in ^{13}C ENDOR studies on CO inhibited nitrogenase),[43] as ENDOR experiments using unlabeled $H^{12}CHO$ show no such signal contributions (see Figure S2).

In Figure 2, the splitting of about 0.6 MHz at both extreme g values changes over the EPR envelope, to about 1.2 MHz in width for broad shoulders, while the maximum intensity narrows to 0.3 MHz at intermediate fields. These variations suggest that the dipolar component is larger than the isotropic component. Simulation of the Q-band ENDOR signal with $\mathbf{A} = [-0.24\ -0.62\ 1.22]$/MHz, consisting of $A_{iso} = 0.12$, $\delta = 0.35$, and $T = 0.55$, where $\mathbf{A} = A_{iso} + T\,[-(1-\delta)\ -(1+\delta)\ 2]$ with Euler angles $(\alpha,\beta,\gamma) = (15, -55, 20)$/deg, represents the field-dependent pattern, but without the orientational distributions that would give rise to low resolution of the shoulders.

Simulations of the Q-band ENDOR data using an approximate local spin model are shown in Figure S3. It was found that the hyperfine values were very weakly dependent on the $\mathbf{g}$ tensor orientation in the molecular frame, and $\Delta\mathbf{g}$ was simply defined by the molecular $\mathbf{g}$ tensor. By these calculations, dipolar components required to fit the shoulders in intermediate fields in Figure 2, i.e., $A_{max} \approx 1.2$ MHz, could arise only through positions of formaldehyde that either bisect the azadithiolate bridge or the positions lying on the side closer to the $[4Fe\text{-}4S]_H^+$ cluster. Alternatively, the description of the delocalized spin projection factors for Fe_p and Fe_d would have to be revised by more than a factor of 3 to fit the 0.6 MHz hyperfine splitting by coordination to the distal Fe site, as is shown in panel E of Figure S3. Using $k_p' = 0.065$ and $k_d' = 0.025$ clearly reduces the dipolar component of the distal iron coordination site to a value that is nearly indistinguishable from matrix formaldehyde.

A third class of ^{13}C is seen with very low intensity in the ENDOR data, a signal is seen at $g = 2.072$ as shoulders at ± 0.5 MHz and at $g = 1.8752$ as slight peaks near ± 0.9 MHz. These features are better resolved as contour level representing 3% of the maximum intensity, just above baseline noise in X-band HYSCORE. Colinearity with the ^{13}C Larmor frequency antidiagonal suggests that the signals are largely isotropic rather than dipolar in character and they can be simulated with $A_{iso} = 1$ MHz, $T = 0.75$ MHz (not shown). However, the intensity is insufficient for detailed analysis.

The skyline projections above the 2-D HYSCORE plots in Figure 3 show the same splitting of ca. 0.6 MHz as in ENDOR,

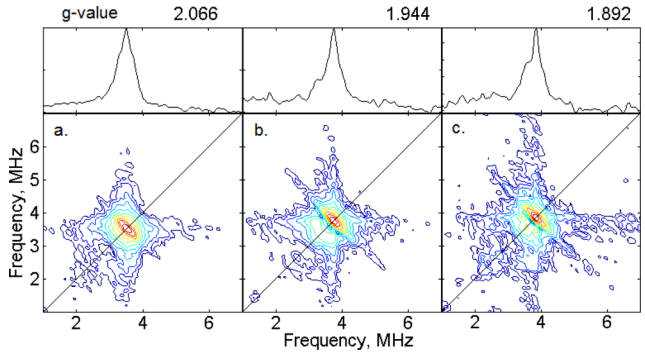

Figure 3. Frequency domain of field-dependent X-band HYSCORE of H_{ox-2} [FeFe]-H2ase with ^{13}C-labeled formaldehyde. Upper panels are skyline projections (summations along vertical axes of lower plots). Data are: (a) at 3275 G, $g = 2.0669$, and $\tau = 144$ ns; (b) at 3482 G, $g = 1.944$, and $\tau = 132$ ns, and (c) at 3576 G, $g = 1.983$, and $\tau = 132$ ns. For all data the microwave frequency was 9.474 GHz, $t_1 = t_2 = 100$ ns, $\pi/2 = \pi = 8$ ns. The spacing of contour lines is 0.3167 on a logarithmic scale.

but here, the signal is dominated by weakly coupled ^{13}C. The asymmetry of the skyline projection and frequency plot suggest underlying signals, such as the large quadrupole interactions of CN^-. By scaling the hyperfine tensor of the ^{14}N in the distal CN^- ligand to 1/10th of the well-defined literature values for the H_{ox} state, signals would be in the same region as ^{13}C, seen in Figure S4. In the H_{ox}-CO form, the hyperfine interactions to ^{13}C of both CN^- ligands are more equivalent than in H_{ox}[44] and the resulting reduction in hyperfine for the distal CN^- ligand leads to ^{14}N signals in the same region as the ^{13}C signals of HCHO in H_{ox-2}[45].

To obtain a picture of the relative amounts of the different species, 3-pulse ESEEM was acquired with DCDO added instead of $H^{13}CHO$, depicted in Figure S5. The modulation depth in the ESEEM data is primarily due to weakly coupled formaldehyde.[46] There is little field dependence to the 3-pulse ESEEM frequency spectra and modulation depth, a case arising when the hyperfine interactions are disordered. Indeed, the data can be fit with two ^{14}N and the hyperfine of the specific ^{13}C, scaled to ^2H, combined with a Gaussian distribution ($\mu = 0.1$, $\sigma = 0.13$ MHz) of six weak ^2H hyperfine interactions that are randomly oriented.

The pulsed-EPR experiments presented herein establish that formaldehyde can access the active site of the H-cluster, and simulations indicate several possible binding sites. A recent study suggested, using site-selective X-ray absorption and emission spectroscopy, that a bridging μ-hydrido ligand between Fe_p and Fe_d might be formed and accumulate in the H_{ox-2} level under conditions similar to our sample preparations, i.e., under H_2 flow without the presence of an external redox partner.[14] Our ENDOR results cannot rule out the existence of

DOI: 10.1021/ja513074m
J. Am. Chem. Soc. 2015, 137, 5381−5389

such a species, however, it is unlikely that it can be a catalytic intermediate of mechanistic relevance, given the recently established requirement for the organic bridging ligand to be adt,[47] an observation that is rationalized by the bridgehead N atom acting as the pendant base, lying in close proximity to Fe_d to cleave H_2 in the manner of a frustrated Lewis pair mechanism. Further, although it would be thermodynamically more stable than its terminal analogue, formation of a bridging hydride seems to be kinetically hindered, as it would require rearrangement of surrounding amino acids at a significant energetic cost. In the [FeFe]-H2ase from *Clostridium pasteurianum* the salt bridge that holds Lys358 in place (Lys358 is conserved in other [FeFe]-H2ases) to form a hydrogen bond to the Fe_d ligated CN^- is stabilized by a binding energy of 99 kcal mol^{-1}.[48]

To help understand how formaldehyde inhibits the *mechanism* of hydrogen formation by [FeFe]-hydrogenases, i.e., the catalytic cycle, we evaluated our EPR results in the context of other experimental and theoretical observations, thus placing realistic chemical constraints on possible binding modes. From PFE experiments[4,9] we know that the rapid binding of formaldehyde under catalytic turnover occurs with τ = 7.89 s at −0.56 V and is fully reversible, and the formaldehyde-inhibited state is fully recovered after 300 s, a time scale similar to our EPR sample preparations (Figure S1). Further, this reversible process exhibits a strong potential dependence, with the most reduced level H_{ox-2} showing the highest degree of inhibition. Taken together with our EPR results that firmly establish the presence of formaldehyde in the vicinity of the H-cluster, these observations strongly suggest that HCHO reacts at a mechanistically important site in the H-cluster, i.e., Fe_d, the likely site of H_2 binding as inferred from CO inhibition studies.[2] If formaldehyde was to react with a hydrido-ligand bound to Fe_d (or bridging between Fe_d and Fe_p), a methoxide species would be formed.[4] However, release of methanol is not detected,[12] and it has recently been proposed that hydride formation only occurs upon reduction of H_{ox-1},[1,15] indicating that formaldehyde is very likely to intercept the H-cluster before formation of a Fe-hydride in the most reduced state of the enzyme. In light of these arguments, we conducted DFT calculations on a likely candidate that may form during turnover, consistent with the above-mentioned restraints.

Density Functional Theory. Scheme 1 highlighted the fact that the precise order of protonation and electronation steps that lead, ultimately, to release of H_2 is uncertain. The lack of methanol detection[4,12] and EPR and ENDOR data now suggest that formaldehyde intercepts the H_{ox-2} level before hydride formation at Fe_d rather than afterward, as assumed in our previous paper,[4] since hydride transfer to the carbonyl-C should produce methoxide. In 2009, Bruschi et al. identified a number of possible intermediates that link H_{ox} and (hydrido-forms of) the H_{ox-2} level including one, "$H_{ox-2}(H^-)$" (Scheme 3) with Fe_d carrying a terminal hydride and adt-N being unprotonated that bears a strong consistency with one of the species responsible for the ^{13}C ENDOR signal and the strong potential dependency of inhibition observed in PFE experiments. The species $H_{ox-2}(H^-)$ is in the H_{ox-2} electronation level, and Fe_d is coordinatively saturated, with a small amount of spin density delocalized onto Fe_d.[8] We therefore used DFT to explore potential modes for formaldehyde binding to Fe_d in the H_{ox-2} level in place of a proton. Our computational protocol followed closely that established by Bruschi et al.[8] in

Scheme 3. Comparison of the Hydrido Species $H_{ox-2}H^-$[8] with the Formaldehyde Adduct II

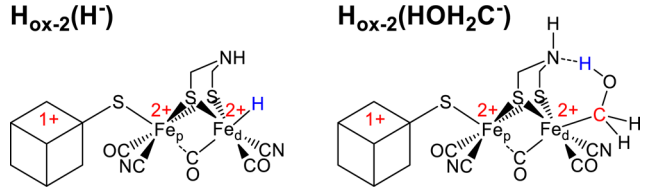

that we took the protein active site from the H-cluster of *Desulfovibrio desulfuricans* and truncated it, as shown in Figure 4, with four methyl carbons frozen at their crystallographic positions. Total energies and Mulliken spin densities for the various stationary points are summarized in Table 1.

Table 1. Total Energies and Mulliken Spin Densities for I and II

	HCHO (**I**)	$^-CH_2OH$ (**II**)	
	BP86	BP86	B3LYP
energy/au	−12501.3804	−12501.9462	−12500.4320
$\langle S^2\rangle$	6.53	6.68	8.01
ρ(Fe1)	3.16	3.11	3.51
ρ(Fe2)	3.12	3.05	3.60
ρ(Fe3)	−2.97	−3.04	−3.44
ρ(Fe4)	−2.69	−2.69	−3.28
$\rho(Fe_p)$	0.02	0.23	0.03
$\rho(Fe_d)$	0.01	0.09	0.01
$\rho(S_{br})$	0.05	0.01	0.04

Introduction of a HCHO unit in the vicinity of the distal iron leads to a rather weakly bound intermediate **I** with Fe−C and Fe−O distances of 2.86 and 3.56 Å, respectively (**I** in Figure 4 and Table 1, above). The formaldehyde is stabilized by a hydrogen bond to the proton on the bridgehead adt-N, but is otherwise not strongly bound. The spin-density on $[2Fe]_H$ is negligible in **I** (<0.03 electrons in total) which is formulated as a $[4Fe\text{-}4S]^{1+}$ species, consistent with the spectroscopically characterized (H_{sred}) form of H_{ox-2}.[15] The net spin densities and values of $\langle S^2\rangle$ suggest that the electronic structure of **I** is well described as an exchange-coupled $[4Fe\text{-}4S]^{1+}$ cluster, and the Kohn−Sham molecular orbitals (Figure S7) confirm this picture. Addition of a proton to the system, i.e., protonation of adt-N, results in a direct Fe−C covalent bond (Fe−C = 2.11 Å) along with transfer of a proton from the bridgehead N atom to the O atom of HCHO (structure **II** in Figure 4). This formation of an Fe_d-C bond, following (the first) protonation of adt-N, leads to a formal two-electron oxidation of the $[2Fe]_H$ unit. The result is the accumulation of a small amount of spin density on Fe_d, consistent with the ENDOR results. We note, however, that the precise value of this spin density is extremely dependent on the computational details and in particular on the exchange functional. Switching from the BP86 functional to the hybrid B3LYP results in accumulation of a larger spin moment on the high-spin Fe centers of the cubane, with a concomitant decrease at the catalytic unit. The uncertainty in the absolute magnitude of the spin density precludes a study of the hyperfine coupling, but the computational study establishes that binding of the HCHO unit via a covalent Fe−C bond is favorable at the highly reduced oxidation levels of interest here, but only when a proton is also present at the bridgehead nitrogen.

DOI: 10.1021/ja513074m
J. Am. Chem. Soc. 2015, 137, 5381−5389

DISCUSSION

The hypothesis we now propose takes into consideration all the observations and data obtained on the formaldehyde inhibition reaction, along with evidence from investigations of others, to arrive at a consistent model. Comparing the structural information obtained from the ^{2}D ESEEM experiments carried out at X-band (Figure S5) to the ^{13}C ENDOR results, it becomes apparent that although there is a specific interaction of formaldehyde with the H-cluster, which is responsible for the isotropic hyperfine interaction and can, among other possibilities, be attributed to direct Fe−C coordination, the whole picture is more complex. The large ^{2}D ESEEM modulation depth suggests that much more "matrix" formaldehyde is present in the vicinity of the active site than is specifically bound. This is not surprising: anhydrous HCHO molecules, being neutral and of similar size to other small molecules such as CO or O_2 that are known to diffuse freely into hydrogenases,[49] should be able to occupy many different sites within the protein.

We note that **I** can be interpreted as being the "limiting case" of a single matrix HCHO (*vide supra*), i.e. a single formaldehyde molecule approaching Fe_d closely, but not yet being bound. As depicted in Figure 4, protonation of adt-N is

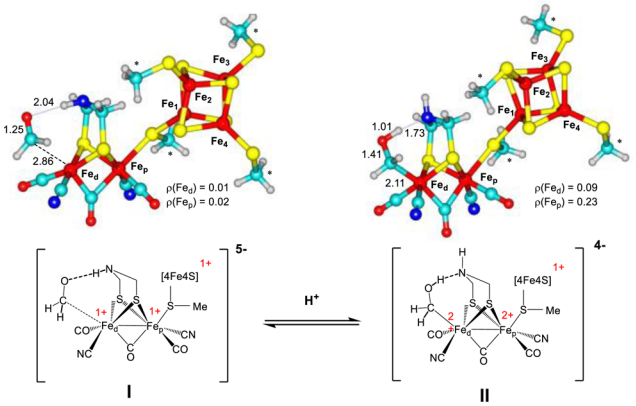

Figure 4. DFT-computed structures for possible adducts of H_{ox-2} and HCHO. Asterisks indicate methyl carbons that are frozen during the geometry optimization process.

required to shift the equilibrium toward **II**. The precise values of the spin density at the distal iron in **II** are somewhat dependent on the details of computational methodology, but lie in the range of 0−0.10 electron, consistent with our EPR data that require the great majority of spins to be localized on $[4Fe\text{-}4S]_H$ (Figure 1). The B3LYP functional which includes exact Hartree−Fock exchange lies at the lower end of this scale, while gradient-corrected functionals (BP86) give larger values. The results reported by Bruschi et al. for the hydrido complex $H_{ox-2}(H^-)$ show very similar trends and very similar absolute values of $\rho(Fe_{p/d})$.[8] Our computational results therefore give rise to the hypothesis that HCHO coordination to the unprotonated Fe_d is favorable provided it is accompanied by protonation at the bridgehead adt-N (the first proton transfer, in our case).

Our results suggest that binding of HCHO, as in structure **II**, results in a state that is equivalent to the hydrido complex, $H_{ox-2}(H^-)$, that exists just before H−H bond formation (Scheme 3). In essence, HCHO has intercepted the catalytic cycle at the point of the first H-transfer from adt-N to Fe_d. This proton, transferring from quaternized adt-N, is abstracted instead by HCHO during formation of the covalent Fe_d-C bond. Structure **II** is best expressed as a carbanionic complex $H_{ox-2}(HOH_2C^-)$ in which HOH_2C^- is a hydride analogue. The stable adduct may also offer protection against more permanent inactivation, if the latter involved attack by formaldehyde on the bridgehead amine-N.

We note here the strong links to existing models for the catalytic cycle where a bridging[14] or, most-likely, terminal hydride (at Fe_d)[48] is formed upon reduction of H_{ox-1} and transfer of the first proton required for H_2 formation from the bridgehead adt-N:[1,8] the subsequent second protonation of adt-N leads to electron transfer from $[4Fe\text{-}4S]_H$ to $[2Fe]_H$. This through-bond reoxidation of $[4Fe\text{-}4S]_H^{1+}$[8] results in the formation of $H_{ox-2}(2H)$ (Scheme 1) which is immediately followed by facile formation and release of H_2.

Structure **II**, which requires only minimal reorganization of the H-cluster, accounts for the rapid and reversible inhibition by formaldehyde. The main mechanistic difference between formaldehyde inhibition and H_2 formation is that the second protonation of **II** at adt-N is not achievable, as the amine group is stabilized through hydrogen bonding with the adjacent hydroxyl group. This aspect explains why in **II**, similar to $H_{ox-2}(H^-)$ and in contrast to $H_{ox-2}(2H)$ (*vide supra*), the majority of unpaired electron density still resides on $[4Fe\text{-}4S]_H$.[8]

In Figure 4, all that is required to release HCHO from the active site is the transfer of the hydroxyl proton back to the bridgehead adt-N. Our proposed mode of inhibition accounts not only for the PFE results but also the subsequent failure to detect any release of methanol. Direct reaction with unprotonated Fe_d in H_{ox-2}, i.e., Fe_d having a vacant coordination site (as opposed to hydride transfer from $H_{ox-2}(H^-)$),[4] is also fully consistent with experimental evidence for H_{ox-1} being unprotonated at Fe_d.[13,14]

Our previous PFE experiments under turnover conditions established that formaldehyde shows a weak affinity for the H_{ox-1} level and a much stronger affinity for H_{ox-2}. This observation strongly indicates that, while the second electronation step to form H_{ox-2} might not be necessary for some minor degree of HCHO inhibition to occur (e.g., through formation of an H_{ox-1} analogue of **I**), significant inhibition by Fe−C bond formation occurs only in the H_{ox-2} level. We can exclude a large population of the H_{ox-1} level since our EPR sample preparation method of prolonged H_2 incubation produces clean H_{ox-2} samples, as established by FTIR spectroscopy.[15]

We cannot exclude the possibility that the state on the H_{ox-2} overall redox level that is inhibited by formaldehyde (leading to structure **II**) measured by EPR differs from the transient state on the same redox level that is formed under catalytic turnover, inhibition of which we have demonstrated by PFE experiments.[4,9] However, while this general restriction applies to all spectroscopic states identified and characterized by various methods (e.g., refs 14, 15, and 20 for the H_{ox-2} level), the combination of experimental and theoretical evidence presented above provides compelling evidence that, under catalytic turnover, formaldehyde inhibits H_2 formation by binding to a highly reduced H-cluster having a vacant coordination site at Fe_d.

To summarize, our results support a model in which Fe−C bond formation in the most reduced state of the H-cluster can only occur if a Fe−H bond has not yet formed, a conclusion

DOI: 10.1021/ja513074m
J. Am. Chem. Soc. 2015, 137, 5381−5389

that has important mechanistic implications. The requirement for secondary stabilization through interaction with the O atom, as seen in simple formaldehyde complexes, is satisfied by use of the pendant-adt-N···H. A new link, both structural and conceptual, is now made between the pendant adt-N and the catalytic Fe_d. Whereas free formaldehyde is a proton mimic, the bound protonated formaldehyde anion, as illustrated in Scheme 3, mimics a terminal hydride just before the point at which a second proton binds to the adt-N, ultimately transferring to form H_2.

■ ASSOCIATED CONTENT

Supporting Information

Supplemental PFE data, EPR spectra and simulations, computational methodology and results. This material is available free of charge via the Internet at http://pubs.acs.org.

■ AUTHOR INFORMATION

Corresponding Authors

*fraser.armstrong@chem.ox.ac.uk
*william.myers@chem.ox.ac.uk
*thomas.happe@rub.de
*john.mcgrady@chem.ox.ac.uk

Notes

The authors declare no competing financial interest.

■ ACKNOWLEDGMENTS

The research was supported by the U.K. BBSRC (BB/L009722/1 and BB/M005720/1) and EPSRC (EP/H019480/1). A.B. thanks St. John's College Oxford for a Graduate Scholarship. F.A.A. is a Royal Society-Wolfson Research Merit Award holder. T.H. acknowledges support from the Deutsche Forschungsgemeinschaft (HA 255/2-1), (DIP Project LU 315/17-1) and the Volkswagen foundation (Az.: 88240). J.E. is supported by the Studienstiftung des deutschen Volkes. W.K.M. is supported by the UK EPSRC (EP/L011972/1, grant to CAESR, the Centre for Advanced Spin Resonance).

■ REFERENCES

(1) Lubitz, W.; Ogata, H.; Rüdiger, O.; Reijerse, E. *Chem. Rev.* **2014**, *114*, 4081.
(2) Lemon, B. J.; Peters, J. W. *Biochemistry* **1999**, *38*, 12969.
(3) Baffert, C.; Bertini, L.; Lautier, T.; Greco, C.; Sybirna, K.; Ezanno, P.; Etienne, E.; Soucaille, P.; Bertrand, P.; Bottin, H.; Meynial-Salles, I.; De Gioia, L.; Léger, C. *J. Am. Chem. Soc.* **2011**, *133*, 2096.
(4) Foster, C. E.; Krämer, T.; Wait, A. F.; Parkin, A.; Jennings, D. P.; Happe, T.; McGrady, J. E.; Armstrong, F. A. *J. Am. Chem. Soc.* **2012**, *134*, 7553.
(5) Stripp, S. T.; Goldet, G.; Brandmayr, C.; Sanganas, O.; Vincent, K. A.; Haumann, M.; Armstrong, F. A.; Happe, T. *Proc. Natl. Acad. Sci. U.S.A.* **2009**, *106*, 17331.
(6) Goldet, G.; Brandmayr, C.; Stripp, S. T.; Happe, T.; Cavazza, C.; Fontecilla-Camps, J. C.; Armstrong, F. A. *J. Am. Chem. Soc.* **2009**, *131*, 14979.
(7) Swanson, K. D.; Ratzloff, M. W.; Mulder, D. W.; Artz, J. H.; Ghose, S.; Hoffman, A.; White, S.; Zadvornyy, O. A.; Broderick, J. B.; Bothner, B.; King, P. W.; Peters, J. W. *J. Am. Chem. Soc.* **2015**, *137*, 1809.
(8) Bruschi, M.; Greco, C.; Kaukonen, M.; Fantucci, P.; Ryde, U.; De Gioia, L. *Angew. Chem., Int. Ed.* **2009**, *48*, 3503.
(9) Wait, A. F.; Brandmayr, C.; Stripp, S. T.; Cavazza, C.; Fontecilla-Camps, J. C.; Happe, T.; Armstrong, F. A. *J. Am. Chem. Soc.* **2011**, *133*, 1282.
(10) Greco, C.; Bruschi, M.; De Gioia, L.; Ryde, U. *Inorg. Chem.* **2007**, *46*, 5911.
(11) Greco, C.; Bruschi, M.; Fantucci, P.; Ryde, U.; De Gioia, L. *ChemPhysChem* **2011**, *12*, 3376.
(12) Foster, C. E. Ph.D. Thesis, University of Oxford, 2012.
(13) Lambertz, C.; Chernev, P.; Klingan, K.; Leidel, N.; Sigfridsson, K. G. V.; Happe, T.; Haumann, M. *Chem. Sci.* **2014**, *5*, 1187.
(14) Chernev, P.; Lambertz, C.; Brünje, A.; Leidel, N.; Sigfridsson, K. G. V.; Kositzki, R.; Hsieh, C.-H.; Yao, S.; Schiwon, R.; Driess, M.; Limberg, C.; Happe, T.; Haumann, M. *Inorg. Chem.* **2014**, *53*, 12164.
(15) Adamska, A.; Silakov, A.; Lambertz, C.; Rüdiger, O.; Happe, T.; Reijerse, E.; Lubitz, W. *Angew. Chem., Int. Ed.* **2012**, *51*, 11458.
(16) Brown, K. L.; Clark, G. R.; Headford, C. E. L.; Marsden, K.; Roper, W. R. *J. Am. Chem. Soc.* **1979**, *101*, 503.
(17) Green, M. L. H.; Parkin, G.; Moynihan, K. J.; Prout, K. *Chem. Commun.* **1984**, 1540.
(18) Gambarotta, S.; Floriani, C.; Chiesi-Villa, A.; Guastini, C. *Organometallics* **1986**, *5*, 2425.
(19) Berke, H.; Bankhardt, W.; Huttner, G.; v. Seyerl, J.; Zsolnai, L. *Chem. Ber.* **1981**, *114*, 2754.
(20) Mulder, D. W.; Ratzloff, M. W.; Shepard, E. M.; Byer, A. S.; Noone, S. M.; Peters, J. W.; Broderick, J. B.; King, P. W. *J. Am. Chem. Soc.* **2013**, *135*, 6921.
(21) Happe, T.; Naber, J. D. *Eur. J. Biochem.* **1993**, *214*, 475.
(22) Kuchenreuther, J. M.; Grady-Smith, C. S.; Bingham, A. S.; George, S. J.; Cramer, S. P.; Swartz, J. R. *PLoS One* 2010, *5*, e15491.
(23) Akhtar, M. K.; Jones, P. R. *Appl. Microbiol. Biotechnol.* **2008**, *78*, 853.
(24) von Abendroth, G.; Stripp, S. T.; Silakov, A.; Croux, C.; Soucaille, P.; Girbal, L.; Happe, T. *Int. J. Hydrogen Energy* **2008**, *33*, 6076.
(25) Esselborn, J.; Lambertz, C.; Adamska-Venkatesh, A.; Simmons', T.; Berggren, G.; Noth, J.; Siebel, J.; Hemschemeier, A.; Artero, V.; Reijerse, E.; Fontecave, M.; Lubitz, W.; Happe, T. *Nat. Chem. Biol.* **2013**, *9*, 607.
(26) Bradford, M. M. *Anal. Biochem.* **1976**, *72*, 248.
(27) Hemschemeier, A.; Melis, A.; Happe, T. *Photosynth. Res.* **2009**, *102*, 523.
(28) Bell, R. P. In *Advances in Physical Organic Chemistry*; Gold, V., Ed.; Academic Press: Oxford, U.K., 1966; Vol. *4*, p 1.
(29) Hilal, S. H.; Bornander, L. L.; Carreira, L. A. *QSAR Comb. Sci.* **2005**, *24*, 631.
(30) Stoll, S.; Schweiger, A. *J. Magn. Reson.* **2006**, *178*, 42.
(31) Nicolet, Y.; Piras, C.; Legrand, P.; Hatchikian, E. C.; Fontecilla-Camps, J. C. *Structure* **1999**, *7*, 13.
(32) Becke, A. D. *Phys. Rev. A* **1988**, *38*, 3098.
(33) Perdew, J. *Phys. Rev. B* **1986**, *33*, 8822.
(34) Schäfer, A.; Huber, C.; Ahlrichs, R. *J. Chem. Phys.* **1994**, *100*, 5829.
(35) Becke, A. D. *J. Chem. Phys.* **1993**, *98*, 5648.
(36) Frisch, M. J., Trucks, G. W.; Schlegel, H. B.; Scuseria, G. E.; Robb, M. A.; Cheeseman, J. R.; Scalmani, G.; Barone, V.; Mennucci, B.; Petersson, G. A.; Nakatsuji, H.; Caricato, M.; Li, X.; Hratchian, H. P.; Izmaylov, A. F.; Bloino, J.; Zheng, G.; Sonnenberg, J. L.; Hada, M.; Ehara, M.; Toyota, K.; Fukuda, R.; Hasegawa, J.; Ishida, M.; Nakajima, T.; Honda, Y.; Kitao, O.; Nakai, H.; Vreven, T.; Montgomery, J. A., Jr.; Peralta, J. E.; Ogliaro, F.; Bearpark, M.; Heyd, J. J.; Brothers, E.; Kudin, K. N.; Staroverov, V. N.; Kobayashi, R.; Normand, J.; Raghavachari, K.; Rendell, A.; Burant, J. C.; Iyengar, S. S.; Tomasi, J.; Cossi, M.; Rega, N.; Millam, M. J.; Klene, M.; Knox, J. E.; Cross, J. B.; Bakken, V.; Adamo, C.; Jaramillo, J.; Gomperts, R.; Stratmann, R. E.; Yazyev, O.; Austin, A. J.; Cammi, R.; Pomelli, C.; Ochterski, J. W.; Martin, R. L.; Morokuma, K.; Zakrzewski, V. G.; Voth, G. A.; Salvador, P.; Dannenberg, J. J.; Dapprich, S.; Daniels, A. D.; Farkas, Ö.; Foresman, J. B.; Ortiz, J. V.; Cioslowski, J.; Fox, D. J. *Gaussian 09*, revision A. 02; Gaussian, Inc.: Wallingford, CT, 2009.
(37) Guigliarelli, B.; Bertrand, P. In *Advances in Inorganic Chemistry*; Sykes, A. G., Ed.; Academic Press: San Diego, CA, 1999; Vol. *47*, p 421.

DOI: 10.1021/ja513074m
J. Am. Chem. Soc. 2015, 137, 5381−5389

(38) Abdalla, J. A. B.; Bowen, A. M.; Bell, S. G.; Wong, L. L.; Timmel, C. R.; Harmer, J. *Phys. Chem. Chem. Phys.* **2012**, *14*, 6526.
(39) Drago, R. S. *Physical Methods for Chemists*; 2nd ed.; Saunders College Publishing: Philadelphia, PA, 1992.
(40) Mouesca, J.-M.; Lamotte, B. *Coord. Chem. Rev.* **1998**, *178*−*180*, 1573.
(41) Mouesca, J. M.; Noodleman, L.; Case, D. A.; Lamotte, B. *Inorg. Chem.* **1995**, *34*, 4347.
(42) Doan, P. E.; Telser, J.; Barney, B. M.; Igarashi, R. Y.; Dean, D. R.; Seefeldt, L. C.; Hoffman, B. M. *J. Am. Chem. Soc.* **2011**, *133*, 17329.
(43) Pollock, R. C.; Lee, H.-I.; Cameron, L. M.; DeRose, V. J.; Hales, B. J.; Orme-Johnson, W. H.; Hoffman, B. M. *J. Am. Chem. Soc.* **1995**, *117*, 8686.
(44) Myers, W. K.; Stich, T. A.; Suess, D. L. M.; Kuchenreuther, J. M.; Swartz, J. R.; Britt, R. D. *J. Am. Chem. Soc.* **2014**, *136*, 12237.
(45) Silakov, A.; Wenk, B.; Reijerse, E.; Albracht, S. P. J.; Lubitz, W. *J. Biol. Inorg. Chem.* **2009**, *14*, 301.
(46) Hoffman, B. M.; DeRose, V. J.; Doan, P. E.; Gurbiel, R. J.; Houseman, A. L. P.; Telser, J. *Biol. Magn. Reson.* **1993**, *13*, 151.
(47) Siebel, J. F.; Adamska-Venkatesh, A.; Weber, K.; Rumpel, S.; Reijerse, E.; Lubitz, W. *Biochemistry* **2015**, *54*, 1474.
(48) Finkelmann, A. R.; Stiebritz, M. T.; Reiher, M. *Chem. Sci.* **2014**, *5*, 215.
(49) Cohen, J.; Kim, K.; King, P.; Seibert, M.; Schulten, K. *Structure* **2005**, *13*, 1321.

DOI: 10.1021/ja513074m
J. Am. Chem. Soc. 2015, 137, 5381−5389